Structural Engineering and Mechanics, *Vol. 49, No. 6 (2014) 727-743*
DOI: http://dx.doi.org/10.12989/sem.2014.49.6.727

Geometrically nonlinear analysis of planar beam and frame structures made of functionally graded material

Dinh-Kien Nguyen[1a], Buntara S. Gan[*2] and Thanh-Huong Trinh[1b]

[1]*Department of Solid Mechanics, Institute of Mechanics, Vietnam Academy of Science and Technology, 18 Hoang Quoc Viet, Hanoi, Vietnam*
[2]*Department of Architecture, College of Engineering, Nihon University, Koriyama, Fukushima-ken, 963-8642 Japan*

(Received February 10, 2013, Revised January 7, 2014, Accepted February 1, 2014)

Abstract. Geometrically nonlinear analysis of planar beam and frame structures made of functionally graded material (FGM) by using the finite element method is presented. The material property of the structures is assumed to be graded in the thickness direction by a power law distribution. A nonlinear beam element based on Bernoulli beam theory, taking the shift of the neutral axis position into account, is formulated in the context of the co-rotational formulation. The nonlinear equilibrium equations are solved by using the incremental/iterative procedure in a combination with the arc-length control method. Numerical examples show that the formulated element is capable to give accurate results by using just several elements. The influence of the material inhomogeneity in the geometrically nonlinear behavior of the FGM beam and frame structures is examined and highlighted.

Keywords: functionally graded material; beam element; geometrical nonlinearity; finite element method

1. Introduction

Geometrically nonlinear analysis of structures is an important topic in the field of structural and solid mechanics, and various geometrically nonlinear problems have been addressed in the well known textbook by Timoshenko and Gere (1961). Due to large displacements inherited in the geometrical nonlinearity, the analytical methods are often difficult in dealing with the nonlinear structures, and a numerical method, especially the finite element method with its versatility in the spatial discretization, is necessary to use instead of. In order to analyze a beam structure undergoes large displacements by the finite element method, a nonlinear beam element which enables to model accurately the nonlinear behavior of the structure is required. Various beam elements for geometrically nonlinear analysis of beam structure can be found in the literature and some of which have been documented in the textbooks on nonlinear finite element analysis (Crisfield 1991, Belytschko *et al*. 2010). The planar nonlinear beam elements are of considerable interest from both

∗Corresponding author, Associate Professor, E-mail: buntara@arch.ce.nihon-u.ac.jp
[a]Research Associate, E-mail: ndkien@imech.ac.vn
[b]Assistant Researcher, E-mail: thanhhuong31@gmail.com

http://www.techno-press.org/?journal=sem&subpage=8 ISSN: 1225-4568 (Print), 1598-6217 (Online)

research and didactic points of view, and they are still the subject of investigation recently (Nguyen 2004, Nanakorn and Vu 2006, Jafari *et al.* 2010, Nguyen 2012). Depending on the choice of reference configuration, the nonlinear beam elements can be classified into three types, the total Lagrangian formulation, the updated Lagrangian formulation and the co-rotational formulation. In the co-rotational formulation which will be adopted herein, the kinematics are described in an element attached local co-ordinate system. The finite element formulation is firstly formulated in this local system, and then transferred to a global system with the aid of transformation matrices. The elements proposed by Hsiao and Huo (1987), Meek and Xue (1996), Pacoste and Eriksson (1977), Nguyen (2012) are some amongst the others co-rotational beam elements for analysis of planar beams and frames which can be cited herewith.

Functionally graded material was initiated by Japanese scientists in Sendai in 1984 (Kozumi 1997) have received much attention from engineers and researchers. FGM is formed by varying percentage of constituents in any desired spatial direction, and as a result the specific physical and mechanical properties of the formed material can be obtained. FGM is being used widely as a structural material, and analysis of structures made of FGM has become an important topic in the field of structural mechanics. A comprehensive list of publications on analyses of FGM structures subjected to different loadings is given in a review paper by Birman and Byrd (2007), only contributions that are most relevant to the present work are addressed below.

Based on the von Kármán plate theory, Praveen and Reddy (1998) derived a plate element for studying the static and dynamic response of FGM plates. Chakraborty *et al.* (2003) employed the solutions of the governing different equations of an FGM Timoshenko beam segment as interpolation functions to formulate a shear deformable beam element for analyzing the thermoelastic behavior of FGM beams. A beam element based on the higher-order shear deformation beam theory for studying the static behavior of FGM beams under ambient temperature has been derived by Kadoli *et al.* (2008). Singh and Li (2009) proposed a model for computing buckling loads of non-uniform axially FGM columns by approximating the column by another one with piecewise uniform geometric and material properties. Taking the shift in position of the neutral axis into account, Kang and Li (2009, 2010) derived expressions for tip displacements of a nonlinear FGM cantilever beam under a tip load or a tip moment. Lee *et al.* (2010) presented a finite element procedure for computing the post-buckling response of FGM plates under compressive and thermal loads. Alshorbagy *et al.* (2011) studied the free vibration of FGM Bernoulli beams with material gradation in axially or transversally direction through the thickness by using the finite element method. Shahba *et al.* (2011) used the static solutions of a homogeneous Timoshenko beam element to formulate the mass and stiffness matrices for computing the critical loads and vibration characteristics of tapered Timoshenko beams made of axially FGM. Using an analytical method, Huang and Li (2011) studied the bucking of axially graded Bernoulli columns with varying cross sections. Fallah and Aghdam (2011) derived the nonlinear governing differential equation for geometrically nonlinear vibration and post-buckling analysis of FGM beams resting on a nonlinear elastic foundation. Kocatürk and Akbaş (2012) presented the post-buckling analysis of an FGM Timoshenko beam subjected to thermal loading by using the total Lagrangian Timoshenko beam formulation.

In this paper, the geometrically nonlinear analysis of planar beam and frame structures made of FGM by using the finite element method is presented. The material property of the structures is assumed to be graded in the thickness direction by a power law distribution. A Bernoulli beam element, taking the shift in the neutral axis position into account, is formulated in the context of the co-rotational formulation. The nonlinear discrete equilibrium equations are solved by using the

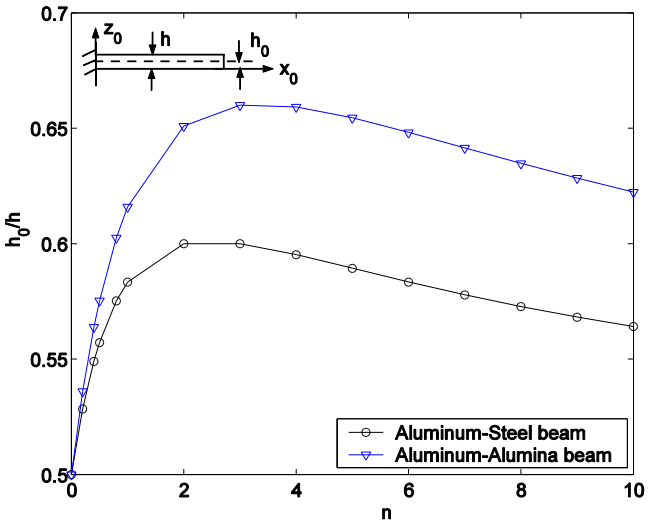

Fig. 1 Power law index versus neutral axis position of FGM beam

incremental/iterative procedure in a combination with the arc-length control method. Numerical examples are given to show accuracy and efficiency of the formulated element and described numerical algorithm. A parametric study is carried out to highlight the influence of the material inhomogeneity on the geometrically nonlinear response of the structures.

2. Neutral axis position

Consider an FGM cantilever beam in a Cartesian coordinate system (x_0, z_0) as depicted in upper left corner of Fig. 1. The beam cross-section is assumed to be uniform rectangular with thickness h and width b. The Cartesian coordinate system (x_0, z_0) is chosen as well as the x_0- and z_0-axes are parallel to the longitudinal direction at the bottom surface and normal to the bottom surface, respectively. The effective Young's modulus of the FGM beam is assumed to vary in the thickness direction by a power law distribution as

$$E(z_0) = E_b + (E_t - E_b)\left(\frac{z_0}{h}\right)^n \tag{1}$$

where E_b and E_t are Young's modulus of the material at the bottom and top surfaces of the beam, respectively; n is the nonnegative power law index, defined the distribution of the constituents. Clearly, due to variation of the effective Young's modulus, the neutral axis is no longer at the midplane, but it shifts from the midplane. The position of the neutral axis can be determined by solving the following equation (Kang and Li 2009, 2010)

$$\frac{E_t - E_b}{E_b}\int_0^1 (1+\beta t)^n t dt + \frac{(1+\beta)^n}{2}\left(1 - \frac{1}{\beta^2}\right) = \frac{E_t - E_b}{E_b}\frac{\Gamma(n+1)}{\beta^2\Gamma(n+3)} \tag{2}$$

where $\Gamma(*)$ is the Gamma function, and $\beta = (h - h_0)/h_0$ with h_0 is the distance from the bottom surface to the neutral axis. The solution of Eq. (2), namely β, depends on E_t/E_b ratio, and the power law index n. The power law index n versus the neutral axis position of is depicted in Fig. 1

for Aluminum-Steel and Aluminum-Alumina beams. The Young's modulus of Aluminum, Steel and Alumina are 70, 210 and 390 GPa, respectively (Praveen and Reddy 1998, Şimşek and Kocatürk 2009).

3. Element formulation

3.1 Co-rotational approach

Co-rotational approach is a convenient way to formulate geometrically nonlinear finite elements. The central idea of the approach is to introduce a local coordinate system that continuously moves and rotates with the element during its deformation process. By using such a local system, the element deformation can be decomposed into rigid body and pure deformation parts, and the geometrically nonlinearity induced by the large body motion is incorporated in transformation matrices. The element formulation is firstly formulated in the local system and then transferred into the global system with the aid of the transformation matrices. Depend on the choice of the local coordinate system, various type of the co-rotational beam elements can be found in the literature. The main points of the co-rotational approach summarized below are closely related to the formulation described by Crisfield (1991), and it has been further developed by Pacoste and Eriksson (1997), and Nguyen (2012).

Fig. 2 shows a planar two-node beam element, (*i*,*j*), and its kinematics in two coordinate systems, a local system ($\bar{x}$, $\bar{z}$), and a global one (*x*, *z*). The element is initially inclined to the *x*-axis an angle θ_0. The global system (*x*, *z*) is fixed, while the local system ($\bar{x}$, $\bar{z}$) is continuously moved and rotated with the element during its deformation process. The local system is chosen as well as its original is always at node *i* and $\bar{x}$-axis directs to node *j*. By choosing such a local system, the axial displacement at node *i* and the transverse displacements at both the two nodes are always zero, $\bar{u}_i = \bar{w}_i = \bar{w}_j = 0$. Thus, the element vector of nodal displacements in the local system contains only three components as

$$\bar{d} = \{\bar{u}_j \;\; \bar{\theta}_i \;\; \bar{\theta}_j\}^T \tag{3}$$

In Eq. (3) and hereafter, a superscript *'T'* denotes the transpose of a vector or a matrix, and the bar

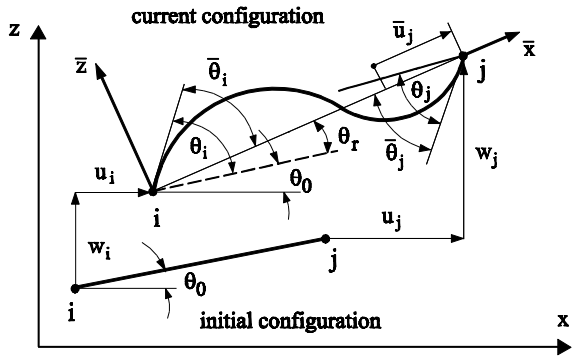

Fig. 2 A co-rotational beam element and its kinematics

suffix is used to indicate a variable or a quantity defined in the local system. The global nodal displacements in general are nonzero, and the element vector of nodal displacements in the global co-ordinate system contains six components as

$$\mathbf{d} = \{u_i \; w_i \; \theta_i \; u_j \; w_j \; \theta_j\}^T \tag{4}$$

The local nodal displacements in Eq. (3) can be computed as (Crisfield 1991)

$$\bar{u}_j = l_n - l; \quad \bar{\theta}_i = \theta_i - \theta_r; \quad \bar{\theta}_j = \theta_j - \theta_r \tag{5}$$

In Eq. (5), l and l_n denote the initial and current lengths of the element

$$\begin{aligned} l &= \sqrt{(x_j - x_i)^2 + (z_j - z_i)^2} \\ l_n &= \sqrt{(x_j + u_j - x_i - u_i)^2 + (z_j + w_j - z_i - w_i)^2} \end{aligned} \tag{6}$$

where (x_i, z_i) and (x_j, z_j) are the co-ordinates of the nodes i and j, respectively; θ_r is the rigid rotation, which can be computed from geometric consideration of Fig. 2 as follows

$$\begin{aligned} \sin\theta_r &= \sin(\theta - \theta_0) = s\, c_0 - c\, s_0 \\ \cos\theta_r &= \cos(\theta - \theta_0) = c\, c_0 + s\, s_0 \end{aligned} \tag{7}$$

where

$$\begin{aligned} c_0 &= \frac{x_j - x_i}{l}, \; s_0 = \frac{z_j - z_i}{l} \\ c &= \frac{x_j + u_j - x_i - u_i}{l_n}, \quad s = \frac{z_j + w_j - z_i - w_i}{l_n} \end{aligned} \tag{8}$$

Provided $|\theta_r < \pi|$, θ_r is given by

$$\begin{aligned} &\theta_r = \sin^{-1}(\sin\theta_r) \text{ if } (\sin\theta_r \geq 0 \text{ and } \cos\theta_r \geq 0) \text{ or } (\sin\theta_r \leq 0 \text{ and } \cos\theta_r \geq 0) \\ &\theta_r = \cos^{-1}(\cos\theta_r) \text{ if } (\sin\theta_r \geq 0 \text{ and } \cos\theta_r \leq 0) \\ &\theta_r = -\cos^{-1}(\cos\theta_r) \text{ if } (\sin\theta_r \leq 0 \text{ and } \cos\theta_r \leq 0) \end{aligned} \tag{9}$$

From Eqs. (5)-(6), one can compute

$$\begin{aligned} \delta\bar{u}_j = \delta l_n &= \frac{(x_j + u_j - x_i - u_i)(\delta u_j - \delta u_i) - (z_j + w_j - z_i - w_i)(\delta u_j - \delta u_i)}{l_n} \\ &= \{-c \quad -s \quad 0 \quad c \quad s \quad 0\}\, \delta\mathbf{d} = \mathbf{r}^T\, \delta\mathbf{d} \end{aligned} \tag{10}$$

Noticing that $\delta\theta_r = \delta\theta$, one can compute $\delta\theta_r$ by differentiation of $\sin\theta$ in Eq. (8) as

$$\delta\theta_r c = -\frac{sc}{l_n}(\delta u_j - \delta u_i) + \frac{c^2}{l_n}(\delta w_j - \delta w_i) \tag{11}$$

So that

$$\delta\theta_r = \frac{1}{l_n}\{s \quad -c \quad 0 \quad -s \quad c \quad 0\}\, \delta\mathbf{d} = \mathbf{z}^T\, \delta\mathbf{d} \tag{12}$$

From Eqs. (5) and (12), the virtual local rotations are given by

$$\delta\bar{\boldsymbol{\theta}} = \begin{Bmatrix} \delta\bar{\theta}_i \\ \delta\bar{\theta}_j \end{Bmatrix} = \left\{ \begin{bmatrix} 0 & 0 & 1 & 0 & 0 & 0 \\ 0 & 0 & 0 & 0 & 0 & 1 \end{bmatrix} - \frac{1}{l_n}\begin{bmatrix} \mathbf{z}^T \\ \mathbf{z}^T \end{bmatrix} \right\} \delta\mathbf{d} = \mathbf{A}^T\, \delta\mathbf{d} \tag{13}$$

Hence the vector of the local virtual nodal displacements relates to that of the global nodal displacements by

$$\delta\bar{\mathbf{d}} = \mathbf{T}\,\delta\mathbf{d} \tag{14}$$

Where the transformation **T** having the form

$$\mathbf{T}=\begin{bmatrix}\mathbf{r}^T\\ \mathbf{A}^T\end{bmatrix}=\begin{bmatrix}-c & -s & 0 & c & s & 0\\ -s/l_n & c/l_n & 1 & s/l_n & -c/l_n & 0\\ -s/l_n & c/l_n & 0 & s/l_n & -c/l_n & 1\end{bmatrix} \tag{15}$$

The internal virtual work for the element can be written in terms of the local and global nodal force vectors as

$$\mathcal{V} = \delta\mathbf{d}^T\mathbf{f}_{in} = \delta\bar{\mathbf{d}}^T\,\bar{\mathbf{f}}_{in} = \delta\mathbf{d}^T\,\mathbf{T}^T\,\bar{\mathbf{f}}_{in} \tag{16}$$

where $\bar{\mathbf{f}}_{in}$ and $\mathbf{f}_{in}$ denote the local and global element internal nodal force vectors associated with the nodal displacement vectors (3) and (4), respectively. Eq. (16) must apply for arbitrary $\delta\mathbf{d}$, so that the global nodal force vector relates to the local one by

$$\mathbf{f}_{in} = \mathbf{T}^T\,\bar{\mathbf{f}}_{in} \tag{17}$$

The element tangent stiffness matrix, $\mathbf{k}_t$, is obtained by differentiation of the internal nodal force vector with respect to the nodal displacements as

$$\delta\mathbf{f}_{in} = \mathbf{k}_t\,\delta\mathbf{d} = \mathbf{T}^T\delta\bar{\mathbf{f}}_{in} + \bar{f}_u\delta\mathbf{T}_1 + \bar{f}_{\theta i}\delta\mathbf{T}_2 + \bar{f}_{\theta j}\delta\mathbf{T}_3 \tag{18}$$

In the above, $\bar{f}_u$, $\bar{f}_{\theta i}$ and $\bar{f}_{\theta j}$ are the local nodal forces corresponding to the local nodal displacements $\bar{u}_j$, $\bar{\theta}_i$ and $\bar{\theta}_j$, respectively; $\mathbf{T}_i$ (i=1..3) are the i^{th} column of the matrix $\mathbf{T}^T$. From Eqs. (10) and (12), we have

$$\delta\mathbf{r} = \mathbf{z}\,\delta\theta_r,\quad \delta\mathbf{z} = -\mathbf{r}\,\delta\theta_r \tag{19}$$

With $\delta\theta_r$ defined by Eq. (12), one gets

$$\delta\mathbf{T}_1 = \frac{\mathbf{z}\,\mathbf{z}^T}{l_n}\,\delta\mathbf{d},\ \ \delta\mathbf{T}_2 = \delta\mathbf{T}_3 = \frac{\mathbf{r}\,\mathbf{z}^T+\mathbf{z}\,\mathbf{r}^T}{l_n^2}\,\delta\mathbf{d} \tag{20}$$

Eqs. (18) and (20) give the element global tangent stiffness matrix as

$$\mathbf{k}_t = \mathbf{T}^T\bar{\mathbf{k}}_t\mathbf{T} + \bar{f}_u\frac{\mathbf{z}\,\mathbf{z}^T}{l_n} + \left(\bar{f}_{\theta i} + \bar{f}_{\theta j}\right)\frac{\mathbf{r}\,\mathbf{z}^T+\mathbf{z}\,\mathbf{r}^T}{l_n^2} \tag{21}$$

where $\bar{\mathbf{k}}_t = \partial\bar{\mathbf{f}}_{in}/\partial\bar{\mathbf{d}}$ is the local tangent stiffness matrix. Eqs. (17) and (21) completely define the global internal nodal vector and tangent stiffness matrix when the local vector, $\bar{\mathbf{f}}_{in}$, and the local stiffness matrix, $\bar{\mathbf{k}}_t$, are known.

3.2 Local formulation

Considering a beam element with length of l in the local system $(\bar{x}, \bar{z})$. Based on Bernoulli beam theory, a degenerated form of Green's strain can be adopted for axial strain in geometrically nonlinear analysis as (Pacoste and Eriksson1997)

$$\epsilon_{xx} = \frac{\partial\bar{u}}{\partial\bar{x}} + \frac{1}{2}\left(\frac{\partial\bar{w}}{\partial\bar{x}}\right)^2 - \bar{z}\frac{\partial^2\bar{w}}{\partial\bar{x}^2} = \epsilon_0 + \bar{z}\,\kappa \tag{22}$$

where $\bar{z}$ is the distance from the considering point to the neutral axis; $\bar{u}$, $\bar{w}$ are the axial and transverse displacements of the point on the neutral axis; $\kappa = -\partial^2\bar{w}/\partial\bar{x}^2$ is the beam curvature. It should be noted that the neutral plane, not the midplane, is chosen as the reference plane herein.

Assuming the linearly elastic behavior, one can write the internal virtual work for the beam element in the form

$$\mathcal{V} = \int_0^l \int_A \sigma_{xx}\delta\epsilon_{xx} dA d\bar{x} = \int_0^l (N\delta\epsilon_0 + M\delta\kappa) d\bar{x} \tag{23}$$

where A is the cross section area; $\sigma_{xx} = E(\bar{z})\epsilon_{xx}$ is the axial stress; N and M are the resultants

$$\begin{aligned} N &= \int_A \sigma_{xx} dA = A_{xx}\epsilon_0 + B_{xx}\kappa \\ M &= \int_A \bar{z}\,\sigma_{xx} dA = B_{xx}\epsilon_0 + D_{xx}\kappa \end{aligned} \tag{24}$$

where A_{xx}, B_{xx} and D_{xx} are the axial, axial and bending coupling, and bending rigidities, respectively, and they are defined as

$$(A_{xx}, B_{xx}, D_{xx}) = \int_A E(\bar{z})(1, \bar{z}, \bar{z}^2) dA \tag{25}$$

In Eq. (25), $E(\bar{z})$ is the effective Young's modulus defined by Eq. (1) with a replacement of z_0 by $\bar{z} = z_0 - h_0$. The integrals in Eq. (25) should be computed in a manner described by Kang and Li (2009), e.g.

$$\begin{aligned} A_{xx} &= \int_A E(\bar{z}) dA = b\left[\int_0^{h-h_0} E(h_0 + \bar{z}) d\bar{z} + \int_0^{h_0} E(h_0 - \bar{z}) d\bar{z}\right] \\ D_{xx} &= \int_A E(\bar{z})\bar{z}^2 dA = b\left[\int_0^{h-h_0} E(h_0 + \bar{z})\bar{z}^2 d\bar{z} + \int_0^{h_0} E(h_0 - \bar{z})\bar{z}^2 d\bar{z}\right] \end{aligned} \tag{26}$$

where b, as above mentioned, denotes the cross section width, and h_0 is the distance from the bottom surface to the neutral axis. In order to derive the local internal force vector and tangent stiffness matrix we need to express the virtual work in terms of the virtual nodal displacements. To this end, the interpolations are necessary to introduce to the displacement field. In the present work, linear and Hermite polynomials are employed to interpolate the axial and transverse displacements, respectively. Noting that $\bar{u}_i = \bar{w}_i = \bar{w}_j = 0$, one can write

$$\bar{u} = N_u \bar{u}_j, \ \bar{w} = \mathbf{N}_w^T \bar{\boldsymbol{\theta}} = N_{wi}\bar{\theta}_i + N_{wj}\bar{\theta}_j \tag{27}$$

where $\bar{\boldsymbol{\theta}} = \{\bar{\theta}_i \quad \bar{\theta}_j\}^T$, and

$$N_u = \frac{\bar{x}}{l}, \ N_{wi} = \left(\bar{x} - 2\frac{\bar{x}^2}{l} + \frac{\bar{x}^3}{l^2}\right), \ N_{wj} = \left(-\frac{\bar{x}^2}{l} + \frac{\bar{x}^3}{l^2}\right), \tag{28}$$

The finite element formulation based on the strain (22) and the interpolation functions (28), however suffers from the membrane locking problem (Crisfield 1991). In order to overcome this problem, the ε_0 in Eq. (22) is replaced by the average strain to ensure a constant membrane strain as (Crisfield 1991, Pacoste and Eriksson 1997)

$$\epsilon_{av} = \frac{1}{l}\int_0^l \epsilon_0 d\bar{x} = \frac{1}{l}\int_0^l \left[\frac{\partial\bar{u}}{\partial\bar{x}} + \frac{1}{2}\left(\frac{\partial\bar{w}}{\partial\bar{x}}\right)^2\right] d\bar{x} \tag{29}$$

Substituting Eqs. (27)-(28) into Eq. (29) and perform the integral, one gets

$$\epsilon_{av} = \frac{1}{l}\bar{u}_j + \frac{1}{30}\left(2\bar{\theta}_i^2 - \bar{\theta}_i\bar{\theta}_j + 2\bar{\theta}_j^2\right) \tag{30}$$

Using the average strain, one can rewrite Eq. (23) in the form

$$\mathcal{V} = \int_0^l \left[N b_u \delta \bar{u}_j + \left(N \mathbf{b}_\theta^T + M \mathbf{c}_w^T \right) \delta \bar{\boldsymbol{\theta}} \right] d\bar{x} \tag{31}$$

where

$$b_u = \frac{\partial N_u}{\partial \bar{x}}, \ \mathbf{b}_\theta = \frac{\partial \epsilon_{av}}{\partial \bar{\boldsymbol{\theta}}} = \frac{1}{30} \begin{Bmatrix} 4\bar{\theta}_i - \bar{\theta}_j \\ 4\bar{\theta}_j - \bar{\theta}_i \end{Bmatrix}, \ \mathbf{c}_w = -\frac{\partial^2 \mathbf{N}_w}{\partial \bar{x}^2} = \begin{Bmatrix} \frac{4}{l} - 6\frac{\bar{x}}{l^2} \\ \frac{2}{l} - 6\frac{\bar{x}}{l^2} \end{Bmatrix} \tag{32}$$

Eq. (31) gives the internal nodal forces in the forms

$$\begin{aligned} \bar{f}_u &= \int_0^l N b_u d\bar{x} \\ \bar{\mathbf{f}}_\theta &= \int_0^l \left(N \mathbf{b}_\theta^T + M \mathbf{c}_w^T \right) d\bar{x} \end{aligned} \tag{33}$$

where $\bar{\mathbf{f}}_\theta$ denotes the local internal nodal force corresponding to the nodal rotations where $\bar{\boldsymbol{\theta}} = \{\bar{\theta}_i \quad \bar{\theta}_j\}^T$.

The local tangent stiffness matrix $\bar{\mathbf{k}}_t$ can be computed by differentiation of the local internal force vector $\bar{\mathbf{f}}_{in}$ with respect to the local nodal displacements (Pacoste and Eriksson 1997), and for the convenience we subdivide $\bar{\mathbf{k}}_t$ into sub-matrices as

$$\bar{\mathbf{k}}_t = \begin{bmatrix} \bar{\mathbf{k}}_{uu} & \bar{\mathbf{k}}_{u\theta} \\ \bar{\mathbf{k}}_{u\theta}^T & \bar{\mathbf{k}}_{\theta\theta} \end{bmatrix} \tag{34}$$

where the sub-matrices are obtained from Eq. (33) as

$$\begin{aligned} \bar{\boldsymbol{k}}_{uu} &= \frac{\partial \bar{f}_u}{\partial \bar{u}} = \int_0^l A_{xx} b_u^2 d\bar{x} \\ \bar{\mathbf{k}}_{u\theta} &= \frac{\partial \bar{f}_u}{\partial \bar{\boldsymbol{\theta}}} = \int_0^l \left(A_{xx} \mathbf{b}_\theta^T + B_{xx} \mathbf{c}_w^T \right) b_u \, d\bar{x} \\ \bar{\mathbf{k}}_{\theta\theta} &= \frac{\partial \bar{\mathbf{f}}_\theta}{\partial \bar{\boldsymbol{\theta}}} = \int_0^l \left(A_{xx} \mathbf{b}_\theta \, \mathbf{b}_\theta^T + 2B_{xx} \mathbf{b}_\theta \, \mathbf{c}_w^T + D_{xx} \mathbf{c}_w \, \mathbf{c}_w^T + N\mathbf{B} \right) d\bar{x} \end{aligned} \tag{35}$$

where **B** is a constant matrix defined as

$$\mathbf{B} = \frac{\partial \mathbf{b}_\theta^T}{\partial \bar{\boldsymbol{\theta}}} = \frac{1}{30} \begin{bmatrix} 4 & -1 \\ -1 & 4 \end{bmatrix} \tag{36}$$

Eqs. (33) and (35) together with Eqs. (17) and (21) completely define the global internal nodal force vector and tangent stiffness matrix.

4. Equilibrium equations

The equilibrium equations for nonlinear analysis of structures are obtained by setting the out-of-balance forces to zeros (Crisfield 1991)

$$\mathbf{g}(\mathbf{p}, \lambda) = \mathbf{q}_{in}(\mathbf{p}) - \lambda \mathbf{f}_{ef} = 0 \tag{37}$$

where the out-of-balance force vector **g** is a function of the current structural nodal displacements **p** and the load-level parameter λ; $\mathbf{q}_{in}$ is the structural internal force vector, constructed from the

element force vector $\mathbf{f}_{in}$ in standard way of the finite element method; $\mathbf{f}_{ef}$ is the fixed external loading vector. The nonlinear Eq. (37) can be solved by an incremental/iterative procedure based on the Newton-Raphson method, in which the norm of vector $\mathbf{g}(\mathbf{p},\lambda)$ is guided towards zero.

In order to trace complete equilibrium paths for possible complex behavior such as snap-through and snap-back, the incremental/iterative procedure is used in a combination with the arc-length method developed by Crisfield (1981, 1991). In the method, the load parameter λ becomes a variable, and a constraint equation is introduced as

$$a = (\Delta\mathbf{p}^T\Delta\mathbf{p} + \Delta\lambda^2\phi^2\mathbf{f}_{ef}^T\mathbf{f}_{ef}) - \Delta l^2 = 0 \tag{38}$$

where Δl is a fixed value chosen by the analyst; the vector $\Delta\mathbf{p}$ and scalar $\Delta\lambda$ are respectively the incremental displacement and load parameter, defined from the last converged state; ϕ is the scaling parameter. For $\phi = 1$, Eq. (38) defines a spherical surface with a radius Δl in the load-displacement space, and it defines a cylindrical surface when $\phi = 0$. With the constrain equation, instead of solving the equilibrium equations (37) directly, we find the intersection of the equilibrium path with the surface defined by Eq. (38). The iterative procedure is obtained from the truncated Taylor expansion of the vector $\mathbf{g}$ and a around the current equilibrium point as

$$\begin{gathered}\mathbf{g} = \mathbf{g}|_0 + \left.\frac{\partial\mathbf{g}}{\partial\mathbf{p}}\right|_0 \delta\mathbf{p} + \left.\frac{\partial\mathbf{g}}{\partial\lambda}\right|_0 \delta\lambda = \mathbf{g}|_0 + \mathbf{K}_t|_0\delta\mathbf{p} + \mathbf{f}_{ef}\delta\lambda = 0 \\ a = a|_0 + 2\Delta\mathbf{p}^T\Delta\mathbf{p} + 2\Delta\lambda\delta\lambda\phi^2\mathbf{f}_{ef}^T\mathbf{f}_{ef} = 0\end{gathered} \tag{39}$$

where $\mathbf{g}|_0$ and $a|_0$ are defined from the current equilibrium point. Eq. (39) gives the iterative displacements $\delta\mathbf{p}$ and iterative load parameter $\delta\lambda$ as

$$\begin{Bmatrix}\delta\mathbf{p} \\ \delta\lambda\end{Bmatrix} = -\begin{bmatrix}\mathbf{K}_t|_0 & \mathbf{f}_{ef} \\ 2\Delta\mathbf{p}^T & 2\Delta\lambda\phi^2\mathbf{f}_{ef}^T\mathbf{f}_{ef}\end{bmatrix}^{-1}\begin{Bmatrix}\mathbf{g}|_0 \\ a|_0\end{Bmatrix} \tag{40}$$

As seen from Eq. (40), the augmented Jacobian matrix within the square brackets in Eq. (40) remains non-singular even when the $\mathbf{K}_t$is singular. However, the Jacobian matrix in (40) is neither symmetric nor banded, and the computation based on the arc-length method is expensive. The cylindrical arc-length method $\phi = 0$ is adopted in the present work. More detail on the arc-length method and its numerical implementation are described by Crisfield (1991).

5. Numerical examples

5.1 Cantilever beam under tip moment

The aim of this study is to verify the accuracy and convergency of the formulated element. To this end, a cantilever beam with total length L = 6 m, width b = 0.15 m and height h = 0.1 m, subjected to a tip moment M is considered. The beam is assumed to be composed from Aluminum and Alumina with Young's modulus stated in Section 2. The problem has been investigated analytically by Kang and Li (2010) with the expressions for the tip displacements are as follow

$$u = \frac{D_{xx}}{M}\sin\left(\frac{M}{D_{xx}}L\right) - L \quad , \quad w = \frac{D_{xx}}{M}\left[1 - \cos\left(\frac{M}{D_{xx}}L\right)\right] \tag{41}$$

where D_{xx} is the effective bending rigidity of the FGM beam, defined in Eq. (25). With the geometric and material data stated above, the effective bending rigidity of the beam, D_{xx} =

3.1483×10^6, 1.2833×10^6, 1.6990×10^6 Nm^2 are obtained for n = 0.5, 1, 3, respectively.

Table 1 lists the tip displacements of the beam with various values of the index n computed by different numbers of the elements. For comparison, the corresponding values of the tip displacements according to Eq. (41) are also given in the Table. As seen from the Table, the formulated element converges very fast to the analytical solutions, and the tip displacements computed by using six elements are the same as that of the analytical method, regardless of the index n and the applied moment. The relation between the tip displacements and the tip moment of the beam for various values of the index n obtained by using six elements is shown in Fig. 3, where the analytical solutions derived by Kang and Li (2010) are depicted by small circles. Again, the figure shows very good agreement between the numerical results of the present work and the analytical solutions derived by Kang and Li (2010).

5.2 Cantilever beam under transverse tip load

In order to study the effect of the material inhomogeneity on the geometrically nonlinear response of the beam and frame structure in more further, the cantilever beam of Subsection 5.1 subjected to a transverse concentrated load P at its free end is analyzed. This problem is stemming from the work by Mattiasson (1981) for a homogeneous beam. Six elements are used to model the beam. In Fig. 4, the tip displacements versus the tip transverse load is depicted for n = 0.5, 1 and 3. As seen from the figure, the displacements are smaller for the beam having a lower index n, regardless of the applied load. This due to the fact that, in refer to Eq. (1), the beam with lower index n contains more Alumina. Since the Young's modulus of Alumina is much higher than that of Aluminum, and thus the beam with lower index n is stiffer. As a result, the beam with lower index n can withstand more external load.

In Fig. 5, the thickness distribution of the axial stress at clamped section is displayed for various values of the index n and the applied load. The effect of the material inhomogeneity is clearly seen from the figure again. Different from homogeneous beams, the axial stress of the

Table 1 Tip displacements of cantilever beam under a tip moment computed by different element numbers

			n_{el}				
$\frac{ML}{E_bI}$	response	n	1	2	4	6	Eq. (41)
3	$\left\|\frac{u}{L}\right\|$	0.5	0.1122	0.1119	0.1119	0.1119	0.1119
		1	0.1868	0.1862	0.1861	0.1861	0.1861
		3	0.3551	0.3531	0.3530	0.3530	0.3530
	$\frac{w}{L}$	0.5	0.3932	0.3933	0.3933	0.3933	0.3933
		1	0.4923	0.4926	0.4926	0.4926	0.4926
		3	0.6285	0.6305	0.6305	0.6305	0.6306
6	$\left\|\frac{u}{L}\right\|$	0.5	0.4059	0.4033	0.4031	0.4031	0.4031
		1	0.6279	0.6230	0.6227	0.6226	0.6226
		3	0.9845	0.9834	0.9834	0.9833	0.9833
	$\frac{w}{L}$	0.5	0.6547	0.6575	0.6576	0.6576	0.6576
		1	0.7110	0.7205	0.7210	0.7211	0.7211
		3	0.6019	0.6447	0.6464	0.6468	0.6468

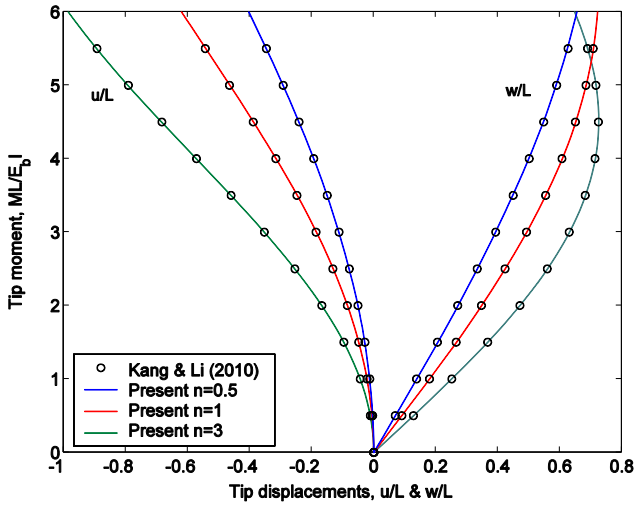

Fig. 3 Relation between tip displacements and tip moment of cantilever beam

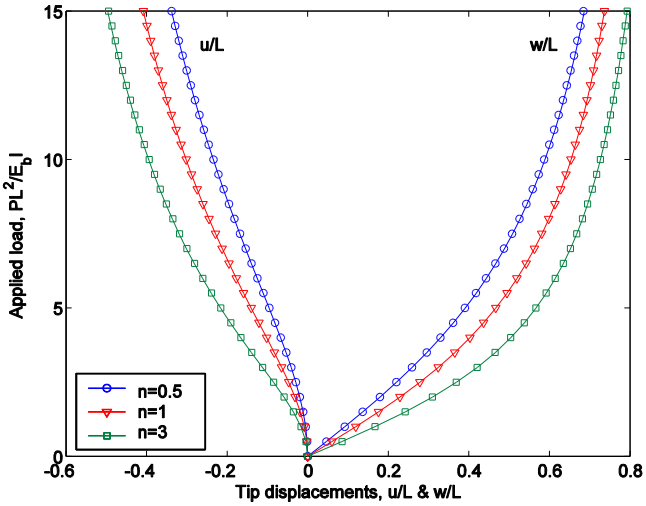

Fig. 4 Relation between tip displacements and tip transverse load of cantilever beam

FGM beam does not vanish at the mid-plane, and the difference between the amplitude of the compressive stress and that of the tensile stress is considerably large, regardless of the applied load. In addition, the axial stress remarkably increases when raising the applied load.

5.3 Asymmetric frame

An asymmetric frame under a concentrated load P as shown in lower part of Fig. 6 is considered. The previous work on the homogeneous frame (Hsiao and Huo 1987, Nguyen 2012) shows that load-displacement curves of the frame exhibit both the snap-back and snap-through behaviors. Thus, this problem is a good example to test the behavior of the beam element and the described numerical algorithm. The frame is assumed to be composed of Aluminum and Steel with

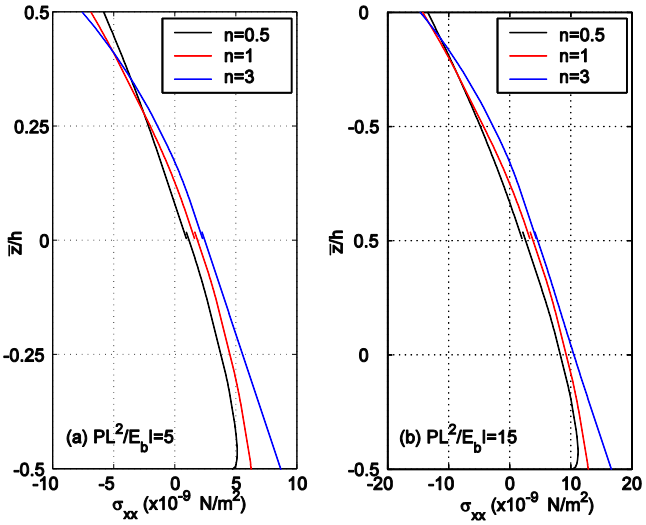

Fig. 5 Thickness distribution of axial stress at clamped end of cantilever beam

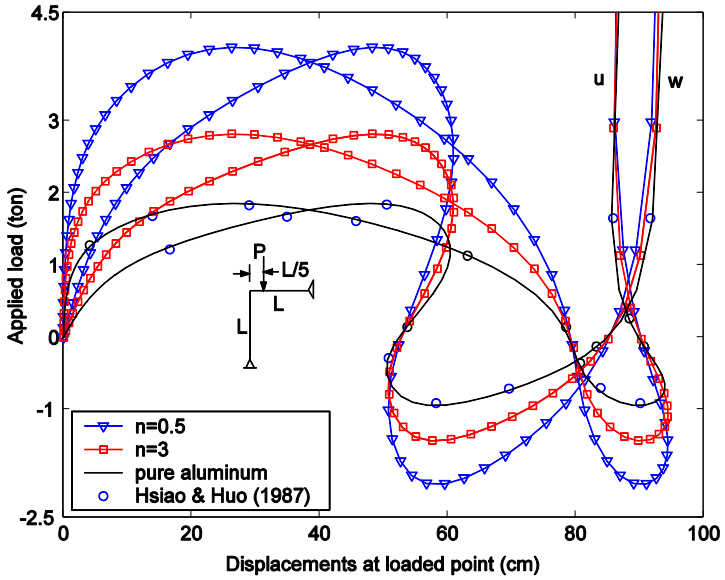

Fig. 6 Load-displacement curves for asymmetric frame

geometric data as follows: L = 120 cm, b = 3 cm and h = 2 cm.

Fig. 6 shows the load-displacement curves for the frame with various values of the index n, where the numerical results computed by Hsiao and Huo (1987) for the pure aluminum frame are depicted by small blue circles. Ten elements, five for each beam have been used to discrete the frame. As seen from the figure, the curves for the pure aluminum frame obtained in the present work are in good agreement with that of Hsiao and Huo (1987). The influence of the material distribution on the behavior of the frame is clearly seen from the figure, and the limit load is higher for a frame having a lower power law index.

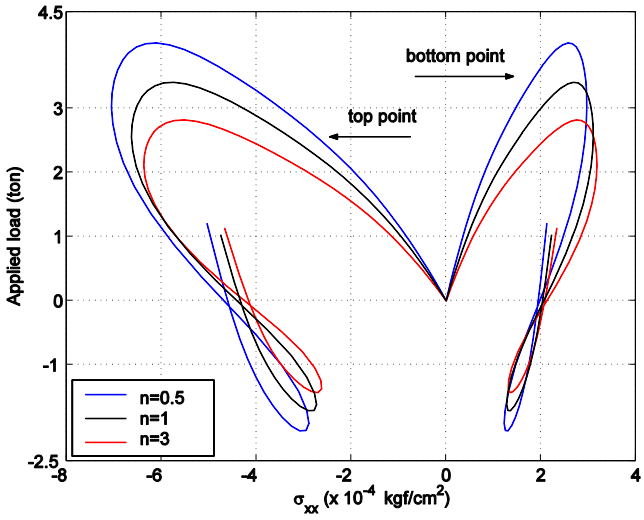

Fig. 7 Axial stress at top and bottom points of loaded section versus applied load for asymmetric frame

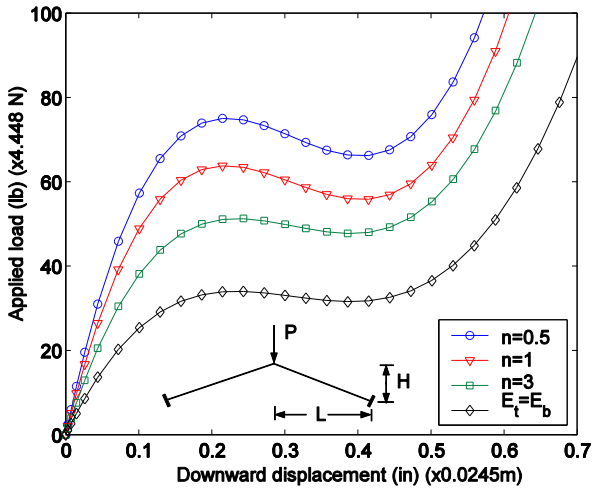

Fig. 8 Load-displacement curves for Williams' toggle frame

The axial stress at the top and bottom points of the loaded section versus applied load of the frame is depicted in Fig. 7 for various values of the index *n*. The stress at the points steadily increases when raising the applied load and it then reaches a limit point as in case of the load-displacement curve in Fig. 6. Since the yield stress of Aluminum is just 2×10^4 kgf/cm^2 (Gere and Timoshenko 1991), plastic deformation will be involved during the loading process. In order to take the effect of the plastic deformation into consideration, an elastic-plastic analysis should be employed as in case of the homogeneous frame (Cichón 1984, Hsiao *et al*. 1988).

5.4 Williams' toggle frame

The Williams' toggle frame shown in lower left corner of Fig. 8, which has been employed by

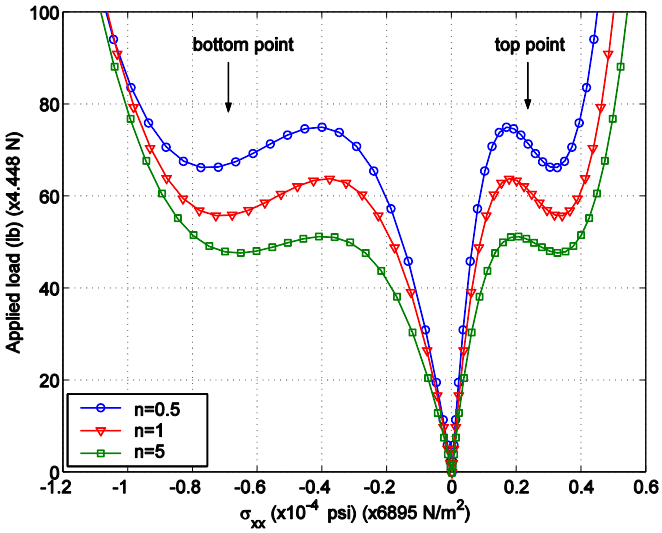

Fig. 9 Axial stress at top and bottom points of clamped section versus applied load of Williams' toggle frame

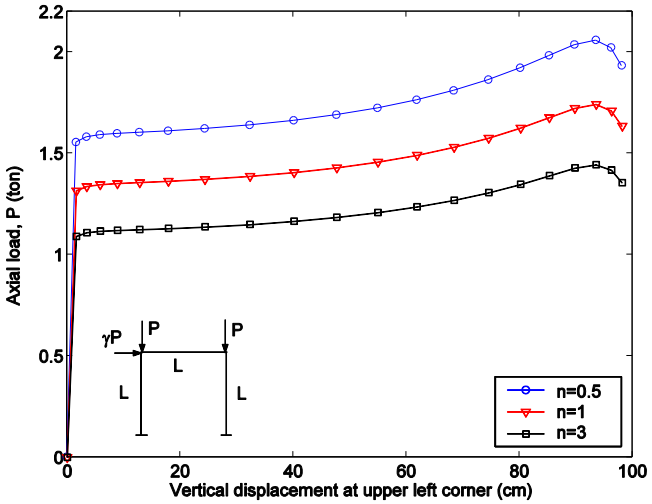

Fig. 10 Load-displacement curves for portable frame

many authors to test their nonlinear beam elements, is considered. The data for computation are as follows: L = 12.943″ (0.329 m), H = 0.386″ (0.01 m), b = 0.753″ (0.019 m), h = 0.243″ (0.006 m), $E_b = 10.3 \times 10^6$ psi (7.1×10^4 MPa), $E_t = 3E_b$. The load-displacement curves for the frame obtained by using six elements, three for each beam, are shown in Fig. 8. The black curve corresponding to a homogeneous frame with $E_t = E_b = 10.3 \times 10^6$ psi is in good agreement with the results in the literature (Pacoste and Eriksson 1997, Nguyen 2012). The effect of the material distribution on the limit load of the FGM frame is clearly seen from the figure, where a lower index n results in a higher limit load. The effect of the material distribution on the behavior of the frame can also be seen from the relation between the axial stress at the top and bottom points of clamped section and the applied load as depicted in Fig. 9.

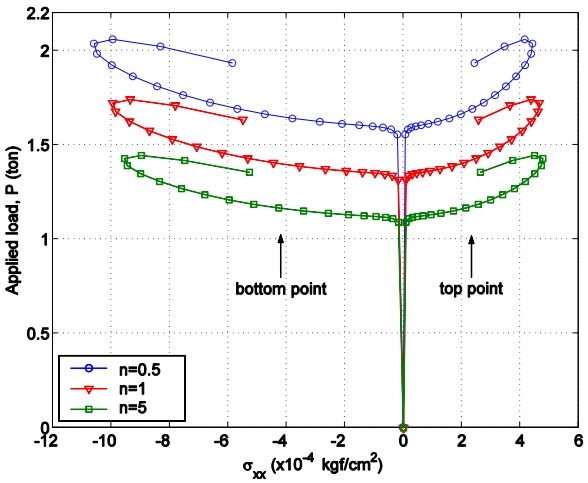

Fig. 11 Axial stress at top and bottom points of upper left corner section versus applied load of portable frame

5.5 Portable frame

A portable frame subjected to load P at its upper corners as shown in the lower left corner of Fig. 10 is analyzed. The frame is assumed to be formed from Aluminum and Steel. The geometric data for computation are L = 120 cm, b = 3 cm, h = 2cm. A small horizontal load γP with γ = 0.001, played as a perturbation, is introduced at the upper left corner. The frame is discretized by six elements, two for each beam. Fig. 10 shows the load-displacement curves for the frame with various values of the index n. As seen from the figure, the index n strongly affects the response of the frame and the limit load is higher for the frame having lower index n.

In Fig. 11, the axial stress at the top and bottom points of upper left corner section versus the applied load of the frame is depicted for various values of the index n. As seen from the figure, the stress gradually increases when raising the applied load; it then follows a snap-back curve after reaching a limit point. The stress, as in case of asymmetric frame, reaches the yield stress when the frame undergoes large displacement. As above mentioned, in order to take the effect of the plastic deformation into account an elastic-plastic analysis should be replaced the elastic analysis used in the present work.

5. Conclusions

A finite element procedure for geometrically nonlinear analysis of planar functionally graded beam and frame structure has been presented. A nonlinear Bernoulli beam element taking the shift in the neutral axis position into account is formulated in the context of the co-rotational formulation. Using the formulated element, the equilibrium paths of the structures have been computed with the aid of the incremental/iterative procedure in a combination with the arc-length control method. A number of numerical examples have been given to show the accuracy and efficiency of the formulated element. The obtained numerical results have shown that the formulated element is capable to give accurate results by using just several elements. The

influence of the material inhomogeneity on the geometrically nonlinear response of the FGM beam and frame structures has been examined and highlighted in detail.

It should be noted that the beam element in the present work was derived based on the Bernoulli assumptions, and thus the effect of shear deformation has not been taken into consideration. The formulated element thus is capable to model the slender beam and frame structures only. In addition, as demonstrated in the numerical examples, the stress at some parts may exceed the yield stress during the structures undergo large displacement, and thus the effect of plastic deformation should be taken into consideration. More work is required to develop a nonlinear beam element which capable to model the shear deformation effect and the elasto-plastic behavior of FGM beam and frame structures.

Acknowledgments

The authors would like to thank Prof. Nguyen Tien Khiem of the Institute of Mechanics, VAST, for his valuable discussion and advice. The financial support from NAFOSTED under project number 107.04.12.09 to the first author is gratefully acknowledged.

References

Alshorbagy, A.E., Eltaher, M.A. and Mahmoud, F.F. (2011), "Free vibration chatacteristics of a functionally graded beam by finite element method", *Appl. Math. Model*., **35**(1), 412-425.

Belytschko, T., Liu, W.K. and Moran, B. (2000), *Nonlinear Finite Elements for Continua and Structures*, John Wiley & Sons, Chichester, USA.

Birman, V. and Byrd, L.W. (2007), "Modeling and analysis of functionally graded materials and structures", *Appl. Mech. Rev.*, **60**(5), 195-216.

Chakraborty, A., Gopalakrishnan, S. and Reddy, J.R. (2003), "A new beam finite element for the analysis of functionally graded materials", *Int. J. Mech. Sci.*, **45**(3), 519-539.

Cichón, C. (1984), "Large displacement in-plane analysis of elastic-plastic frames", *Comput. Struct.*, **19**(5-6), 737-745.

Crisfield, M.A. (1981), "A fast incremental/iterative solution procedure that handles 'snap-through'", *Comput. Struct*., **13**(1-3), 55-62.

Crisfield, M.A. (1991), *Nonlinear Finite Element Analysis of Solids and Structures*, Volume 1, Essentials, John Wiley & Sons, Chichester, USA.

Fallah, A. and Aghdam, M.M. (2011), "Nonlinear free vibration and post-buckling analysis of functionally graded beams on nonlinear elastic foundation", *Eur. J. Mech. A/Solids*, **30**(4), 571-583.

Gere, G.M. and Timoshenko, S.P. (1991), *Mechanics of Materials*, Third SI Edition, Chapman & Hall, London, UK.

Hsiao, K.M. and Huo, F.Y. (1987), "Nonlinear finite element analysis of elastic frames", *Comput. Struct*., **26**(4), 693-701.

Hsiao, K.M., Huo, F.Y. and Spiliopoulos, K.V. (1988), "Large displacement analysis of elasto-plastic frames", *Comput. Struct*., **28**(5), 627-633.

Huang, Y. and Li, X.F. (2011), "Buckling analysis of non-uniform and axially graded beams with varying flexural rigidity", *ASCE J. Eng. Mech*., **137**(1), 73-81.

Jafari, V., Vahdani, S.H. and Rahimian, M. (2010), "Derivation of the consistent flexibility matrix for geometrically nonlinear Timoshenko frame finite element", *Finite Elem. Anal. Des*., **46**(12), 1077-1085.

Kadoli, R., Akhtar, K. and Ganesan, N. (2008), "Static analysis of functionally graded beams using higher

order shear deformation beam theory", *Appl. Math. Model*., **32**(12), 2509-2525.
Kang, Y.A. and Li, X.F. (2009), "Bending of functionally graded cantilever beam with power-law nonlinearity subjected to an end force", *Int. J. Nonlin. Mech*., **44**(6), 696-703.
Kang, Y.A. and Li, X.F. (2010), "Large deflection of a nonlinear cantilever functionally graded beam", *J. Reinf. Plast. Comp*., **29**(4), 1761-1774.
Kocatürk, T. and Akbaş, S.D. (2012), "Post-buckling analysis of Timoshenko beams made of functionally graded material under thermal loading", *Struct. Eng. Mech*., **41**(6), 775-789.
Koizumi, M. (1997), "FGM activities in Japan", *Compos. Part B Eng*., **28**(1-2), 1-4.
Lee, Y.Y., Zhao, X. and Reddy, J.N. (2010), "Postbuckling analysis of functionally graded plates subjected to compressive and thermal loads", *Comput. Meth. Appl. Mech. Eng*., **199**(25-28), 1645-1653.
Mattiasson, K. (1981), "Numerical results for large deflection beam and frame problems analyzed by meams of elliptic integrals", *Int. J. Numer. Eng*., **17**(1), 145-153.
Meek, J.L. and Xue, Q. (1996), "A study on the instability problem for 2D-frames", *Comput. Meth. Appl. Mech. Eng*., **136**(3-4), 347-361.
Nanakorn, P. and Vu, L.N. (2006), "A 2D field-consistent beam element for large displacement analysis using the total Lagrangian formulation", *Finite Elem. Anal. Des*., **42**(14), 1240-1247.
Nguyen, D.K. (2004), "Post-buckling behavior of beam on two-parameter elastic foundation", *Int. J. Struct. Stab. Dyn*., **4**(1), 21-43.
Nguyen, D.K. (2012), "A Timoshenko beam element for large displacement analysis of planar beams and frames", *Int. J. Struct. Stab. Dyn*., **12**(6), 1-9.
Pacoste, C. and Eriksson, A. (1997), "Beam elements in instability problems", *Comput. Methods Appl. Mech. Eng*., **144**(1-2), 163-197.
Praveen, G.N. and Reddy, J.N. (1998), "Nonlinear transient thermoelastic analysis of functionally graded ceramic-metal plates", *Int. J. Solids Struct*., **35**(33), 4457-4476.
Shahba, A., Attarnejad, R., Marvi, M.T. and Hajila, S. (2011), "Free vibration and stability analysis of axially functionally graded tapered Timoshenko beams with classical and non-classical boundary conditions", *Compos. Part B Eng*., **42**(4), 801-808.
Şimşek, M. and Kocatürk, T. (2009), "Free and forced vibration of a functionally graded beam subjected to a concentrated moving harmonic load", *Compos. Struct*., **90**(4), 465-473.
Singh, K.V. and Li, G. (2009), "Buckling of functionally graded and elastically restrained nonuniform column", *Compos. Part B Eng*., **40**(5), 393-403.
Timoshenko, S.P. and Gere, J.M. (1961), *Theory of Elastic Stability*, McGraw-Hill, New York, USA.